Available online at www.sciencedirect.com
SCIENCE DIRECT®
ELSEVIER
International Journal of Solids and Structures 43 (2006) 3166–3184
INTERNATIONAL JOURNAL OF SOLIDS and STRUCTURES
www.elsevier.com/locate/ijsolstr

Analysis of microstructural strain tensors for granular assemblies

Katalin Bagi *

Research Group for Computational Structural Mechanics, Hungarian Academy of Sciences, Department of Structural Mechanics, Budapest University of Technology and Economics, Müegyetem rkp. 3. K.mf.35, H-1521 Budapest, Hungary

Received 10 February 2005; received in revised form 5 July 2005
Available online 8 September 2005

Abstract

The micromechanical interpretation of strain tensor for granular assemblies has been a subject of considerable scientific interest in recent years. This paper gives an overview on 10 different microstructural strain definitions that can be found in the granular mechanics literature. After a theoretical introduction and comparison, the different versions are compared to each other and to the macro-level strain with the help of discrete element simulations.

Keywords: Discrete mechanics; Kinematics; Translation gradient tensor; Numerical simulations

1. Introduction

Strain is a fundamental concept in classical continuum mechanics. Several versions are known such as left or right Cauchy-Green strain tensor, Piola deformation tensor, Green-Lagrange strain tensor, Euler–Almansi strain etc. However, all these versions can be expressed in terms of the gradient tensor of the translation field that is based on the initial geometry (see, for instance, Holzapfel (2001)): the translation gradient tensor plays a basic role in all continuum theories. The translation gradient is also fundamental in the non-classical theories such as Cosserat or Mindlin theories.

The different continuum-mechanical strains intend to characterize the deformations of an infinitesimally small representative volume element around the analyzed point of a continuous domain. Granular assemblies, on the other hand, consist of individual grains of finite size, each of them having their own translational and rotational degrees of freedom. These displacements are strongly heterogeneous: their size and

* Tel.: +36 14631160; fax: +36 14631099.
E-mail address: kbagi@mail.bme.hu

0020-7683/$ - see front matter
doi:10.1016/j.ijsolstr.2005.07.016

magnitude may significantly vary from grain to grain. So the particle translations cannot be estimated as a continuously differentiable translation field.

Establishing a link between particle-level displacements and macro-level deformations is important for those researchers who intend to develop micromechanically based constitutive theories, as well as for those investigators who want to interpret the results of their discrete element simulations from a macro-level context.

There exist many different ideas to interpret the strain tensor from a microstructural point of view. Most of them belong to one of the following two approaches:

(1) Strains based on an equivalent continuum:
In these approaches the assembly is replaced by a continuous domain, and a suitable translation field is assigned to it in such a way that the translations of the characteristic points of the equivalent continuum be equal to the translations of the particle centers. The gradient of this translation field is then determined, and expressed in terms of the particle displacements and the microlevel geometrical characteristics. The different versions deviate from each other in the definition of the equivalent continuum.
(2) Best-fit strains:
In these versions a translation gradient tensor is found that gives the smallest deviation from the characteristic displacements of the system. Depending on the kind of displacement to be approximated, different versions of best-fit strains are gained.

The aim of this paper is to give an overview on these approaches, and to evaluate how closely they approximate the macro-level deformations of the analyzed assembly. While the description of the influence of the microstructure on the overall deformations (and the modification of the microstructure during deformation) is an important fundamental question, from the perspective of practical application it is even more important to analyze whether the different strain versions are in a good agreement with the overall deformations of the assembly.

Section 2 introduces 10 different microstructural strain tensors. Section 3 presents the results of discrete element simulations on their behavior, and Section 4 contains the most important conclusions.

2. An overview of the existing microstructural strain tensors

2.1. Notations and basic assumptions

The analyzed assemblies must contain at least three grains in the case of 2D analysis, and at least four grains in 3D analysis. All strain versions are based on small displacements of the particles, and on the geometry that is valid at the beginning of the displacements.

The particle displacements are characterized in terms of the translations of the particle centers, and the rigid-body rotations of the grains around their centers. The detailed description of the deformations of the particles is not included in the analysis: instead, the deformations are assumed to be restricted to the small neighborhood of the contacts.

Let $\mathrm{d}u_i^p$ denote the translation of the centre of particle p, while $\mathrm{d}\omega_i^p$ is the rigid-body-like rotation of p about its centre. The notation 'd' expresses that these displacements are small. Particles p and q touch each other in contact c, the material points pc and qc (belonging to particles p and q, respectively) form the contact. The contact vectors r_i^{pc} and r_i^{qc} point from the particle centers to the contact. The translation of pc and qc are

$$\mathrm{d}u_i^{pc} = \mathrm{d}u_i^p + \varepsilon_{ijk} r_j^{pc} \mathrm{d}\omega_k^p, \tag{1}$$

$$\mathrm{d}u_i^{qc} = \mathrm{d}u_i^q + \varepsilon_{ijk} r_j^{qc} \mathrm{d}\omega_k^q. \tag{2}$$

(Here ε_{ijk} is the permutation symbol.) The contact deformation is understood as the relative translation of pc and qc (p is the 'first' and q is the 'second' entity of the contact)

$$\mathrm{d}v_i^c = \mathrm{d}u_i^{qc} - \mathrm{d}u_i^{pc} = \mathrm{d}u_i^q + \varepsilon_{ijk} r_j^{qc}\,\mathrm{d}\omega_k^q - \mathrm{d}u_i^p - \varepsilon_{ijk} r_j^{pc}\,\mathrm{d}\omega_k^p. \tag{3}$$

Finally, $\mathrm{d}e_{ij}$ denotes the left gradient of the vector field $\mathrm{d}u_i$: $\mathrm{d}e_{ij} = \mathrm{d}u_j/\mathrm{d}x_i$.

2.2. Strains based on an equivalent continuum

2.2.1. The strain of Bagi

The strain proposed in Bagi (1993, 1996) is valid for 2D or 3D analysis of particles with arbitrary convex shape. The definition is based on the equivalent continuum formed by the *space cells* of the system. The space cells are triangles in 2D and tetrahedra in 3D, formed by the centers of neighboring (but not necessarily contacting) particles (see Fig. 1). The boundary of this equivalent continuum goes through the centers of boundary particles.

A continuous translation field is assigned to this equivalent continuum in the following way. The translations of the nodes are, by definition, equal to the translations of the corresponding particle centers. In any other point of a cell the translation is defined by the linear interpolation of the nodal translations. (Note that inside of a cell the translation field is continuously differentiable, and its gradient is constant within the cell.)

Let $\mathrm{d}\bar{e}_{ij}^L$ denote the (constant) left gradient of the translation field in cell L. Its volume average for the whole domain is

$$\mathrm{d}\bar{e}_{ij} = \frac{1}{V}\sum_{(L)} V^L\,\mathrm{d}\bar{e}_{ij}^L \quad \text{in 3D}, \tag{3a}$$

$$\mathrm{d}\bar{e}_{ij} = \frac{1}{A}\sum_{(L)} A^L\,\mathrm{d}\bar{e}_{ij}^L \quad \text{in 2D}, \tag{3b}$$

where V^L is the volume (in 2D A^L is the area) of the Lth cell, and V is the sum of the volume (A is the total area) of all the cells. The translation gradient $\mathrm{d}\bar{e}_{ij}^L$ can be expressed with the help of a surface integral

$$\mathrm{d}\bar{e}_{ij}^L = \frac{1}{V^L}\oint_{(S^L)} \mathrm{d}u_j n_i\,\mathrm{d}S \tag{4a}$$

or in 2D analysis

$$\mathrm{d}\bar{e}_{ij}^L = \frac{1}{A^L}\oint_{(l^L)} \mathrm{d}u_j n_i\,\mathrm{d}l. \tag{4b}$$

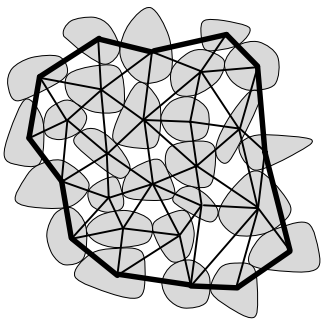

Fig. 1. The space cells.

Here V^L and A^L are the volume or area of space cell L, $\mathrm{d}u_i$ is the translation vector of the boundary point, and n_i is the outwards unit normal vector of the boundary of the cell in the same point. The integration is carried out along the closed boundary surface S^L in 3D, or along the boundary line l^L in 2D. Applying (4), the volume average in (3) can be expressed in terms of the $\mathrm{d}\Delta u_j^c = \mathrm{d}u_j^q - \mathrm{d}u_j^p$ relative translations of the pairs of grains forming the branches of the space cells

$$\mathrm{d}\bar{e}_{ij} = \frac{1}{V}\sum_{(c)} \mathrm{d}\Delta u_j^c d_i^c, \tag{5}$$

where d_i^c is the complementary area vector belonging to the c the pair of grains (Bagi, 1995, 1996), a geometrical characteristic of the local neighborhood of the particle pair. (The details of the derivation can be found in Bagi (1996).) The complementary area vector can be thought of as the dual variable of the branch vector in the sense that if the scalar product of the branch vector and the complementary area vector is determined for every branch of the equivalent continuum, and then these products are summed, the total volume (area in 2D) of the analyzed domain can be determined

$$V = \sum_{(c)} \frac{1}{3}(l_i^c d_i^c) \quad \text{or} \quad A = \sum_{(c)} \frac{1}{2}(l_i^c d_i^c) \tag{6}$$

The antisymmetric part of the tensor $\mathrm{d}\bar{e}_{ij}$ is the average rigid-body-like rotation of the cells, and its symmetric part expresses the average deformation of the equivalent continuum. Hence the symmetric part of (5) is, by definition, the microstructural strain tensor of the analyzed assembly.

Note that in 3D the volume average in (3) can be expressed as a surface integral

$$\mathrm{d}\bar{e}_{ij} = \frac{1}{V}\oint_{(S)} \mathrm{d}u_j n_i \,\mathrm{d}S \quad \text{in } 3D, \quad \text{and} \tag{7}$$

$$\mathrm{d}\bar{e}_{ij} = \frac{1}{A}\oint_{(l)} \mathrm{d}u_j n_i \,\mathrm{d}l \quad \text{in } 2D. \tag{8}$$

Here V and A are the total volume or area of the applied equivalent continuum, $\mathrm{d}u_i$ is the translation of a boundary point where n_i is the outwards unit normal. The integration is carried out along the closed boundary of the whole equivalent continuum. Fig. 2 illustrates the 2D case and the geometrical quantities applied in (8).

2.2.2. The Kruyt–Rothenburg strain

The next microstructural strain appeared as early as 1980 in the Ph.D dissertation of L. Rothenburg (1980), but it was published only sixteen years later, in Kruyt and Rothenburg (1996).

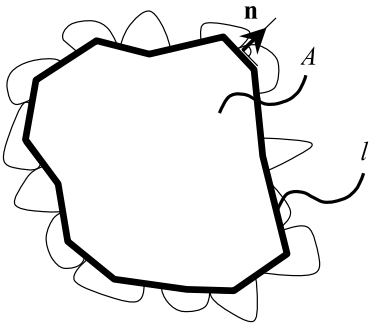

Fig. 2. The geometrical characteristics of the equivalent continuum of the Bagi strain in 2D.

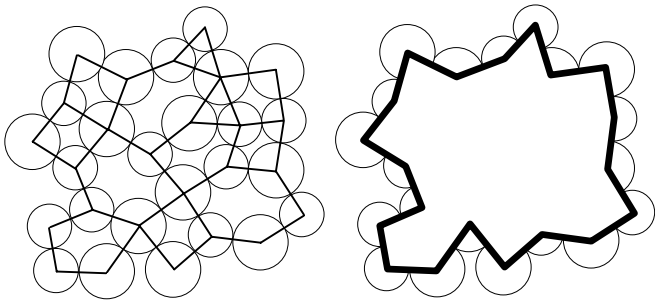

Fig. 3. The Kruyt–Rothenburg equivalent continuum.

The definition is valid for 2D assemblies of particles with any convex shape. It is based on the equivalent continuum illustrated in Fig. 3: the branches connecting the centers of contacting particles determine those polygons whose union gives the equivalent continuum. Its nodes are the particle centers, and its boundary is a zigzag line going through the centers of boundary grains.

A continuous translation field is defined on this equivalent continuum in such a way that in any node the translation vector is equal to the translation of the corresponding particle centre; and linear along the branches between contacting grains. The field is not defined in the interior of the polygons. The exact data of the field will not be necessary; only the existence of a continuous field is assumed.

The average translation gradient of polygon L can be expressed with the help of (4b) as a boundary integral along the boundary line of cell L. In order to derive an expression for the average translation gradient for the whole domain in terms of relative particle translations, the authors introduced the rotated polygon vector, g_i^{pq}, that belongs to the contact formed by particles p and q. If the pq branch is between two neighboring polygons, then it connects the centers of the two polygons; and if pq is on the boundary of the equivalent continuum, then g_i^{pq} connects the centre of the polygon and the centre of the pq boundary branch (see Fig. 4). Its direction is also uniquely defined in Kruyt and Rothenburg (1996).

The polygon vector h_i^{pq} is obtained by a positive rotation over 90° of g_i^{pq}

$$h_i^{pq} = -\varepsilon_{ij} g_j^{pq}. \tag{9}$$

($\varepsilon_{12} = +1, \varepsilon_{21} = -1$ and $\varepsilon_{11} = \varepsilon_{22} = 0$).

Let c denote the contact formed by p and q. Note that if the scalar product of the branch vector and the polygon vector is determined in every contact, and then these products are summed up, the total area of the equivalent continuum can be determined

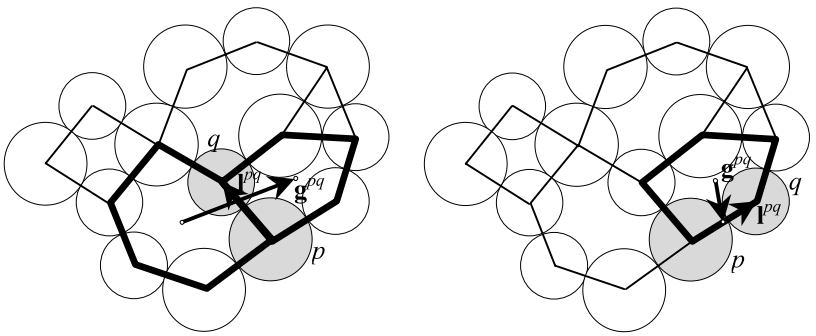

Fig. 4. The rotated polygon vector.

$$A = \sum_{(c)} \frac{1}{2}(l_i^c h_i^c). \tag{10}$$

So the polygon vector plays the same role in the Kruyt–Rothenburg equivalent continuum as the complementary area vector in the 2D version of the previous equivalent continuum consisting of triangles.

Applying the polygon vector, Kruyt and Rothenburg succeeded to express the average translation gradient in the following discrete form:

$$\mathrm{d}\bar{e}_{ij} = \frac{1}{V} \sum_{(c)} \mathrm{d}\Delta u_j^c h_i^c, \tag{11}$$

where the summation is carried out over all contacting pairs of particles, and where the vector $\mathrm{d}\Delta u_i^c$ is the relative translation of the two particle centers. The symmetric part of the tensor (11) is the Kruyt–Rothenburg strain.

Note that the Kruyt–Rothenburg strain and the 2D version of the Bagi strain are equal if the boundaries of the two equivalent continua coincide.

2.2.3. The strain of Kuhn

The next version of strain, proposed by Kuhn (1997, 1999), is also valid for two-dimensional assemblies of convex grains. The equivalent continuum is practically the same as in the case of the Kruyt–Rothenburg strain (the only difference is that only those particles are considered that take part in the load-bearing framework). Defining a translation field in the same way as in case of the Kruyt–Rothenburg strain, the average translation gradient in polygon L can be expressed in terms of the relative translations of contacting grains

$$\mathrm{d}\bar{e}_{ij}^L = \frac{1}{A^L} \sum_{(k_1,k_2)} \frac{Q^{k_1 k_2}}{6} \mathrm{d}\Delta u_j^{k_1} b_i^{k_2}. \tag{12}$$

Here $\mathrm{d}\Delta u_i^{k_1}$ is the relative translation of the two particle centers that form the k_1 edge of the polygon, $b_i^{k_2}$ is an outwards normal vector to edge k_2, with a length that is equal to the length of the k_2 edge (see Fig. 5), A^L is the area of the polygon, and $Q^{k_1 k_2}$ is a multiplier whose exact definition can be found in Kuhn (1999) for different possible cases.

The area-weighted average of these translation gradients gives the average translation gradient for the whole equivalent continuum

$$\mathrm{d}\bar{e}_{ij} = \sum_{(L)} A^L \bar{e}_{ij}^L = \frac{1}{6} \sum_{(L)} \left(\sum_{(k_1,k_2)} Q^{k_1 k_2} \mathrm{d}\Delta u_j^{k_1} b_i^{k_2} \right). \tag{13}$$

Its symmetric part is the average microstructural strain proposed by Kuhn.

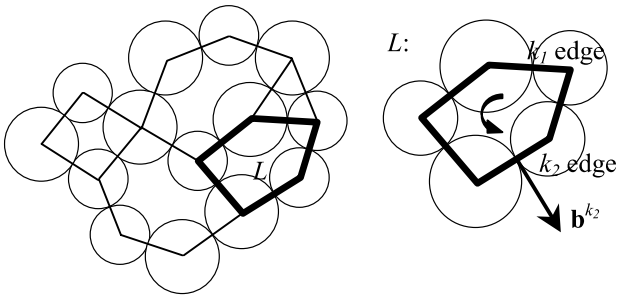

Fig. 5. The Kuhn polygons.

Since the boundaries of the equivalent continua of the Kruyt–Rothenburg strain and of the Kuhn strain are the same, and since the translation field is defined in the same way, the meaning of (11) and (13) is the same and hence the two strains are equal.

2.2.4. The equivalent-continuum strain of Cambou et al.

Another equivalent continuum strain was proposed by Cambou et al. (2000) and Dedecker et al. (2000), also for 2D analysis. In this definition the particles are non-equal circles (though the definition can be generalized for particles having any convex shape). The equivalent continuum consists of triangles formed by the branches between the centers of neighboring (not necessarily contacting) particles. To get these triangles, first the polygons that are formed by those branches connecting the centers of contacting grains have to be prepared. Then the polygons are divided into triangles with the help of their diagonals. (The subdivision into triangles can be done in many alternative ways; all of them lead to the same result.)

A continuous translation field is assigned to this equivalent continuum in a manner similar to that in the case of the Bagi strain. The translations in the nodes are equal to the translations of the particle centers; the translations along the edges and in the interior of the cells are defined by linear interpolation of the nodal translations. The translation field is linear within every triangle, so a constant gradient can be assigned separately to every cell. The area-weighted average of these gradients can be expressed in terms of the relative translations between neighboring particle centers

$$\mathrm{d}\bar{e}_{ij} = \frac{2}{3A}\sum_{(L)} A^L \left(\sum_{s=1}^{3} \mathrm{d}\Delta u_j^s y_i^s \right), \tag{14}$$

where the index L spans the list of triangles, and index s spans the triad of edges of triangle L. The vector $\mathrm{d}\Delta u_j^s$ is the relative translation between the two grains forming edge s. Vector y_i^s is a geometrical characteristic that can be determined with the help of the location of the nodes (see Cambou et al., 2000 for details).

The symmetric part of the tensor in (14) is the equivalent-continuum strain of Cambou et al.

The meaning of (14) is the average translation gradient for a translation field that satisfies the requirements of Kruyt and Rothenburg

- the translations in the nodes of the polygons are equal to the translations of the particle centers;
- the translation field is linear along the polygon edges;
- the translation field is continuous in the whole domain.

Consequently, the equivalent continuum strain of Cambou et al. is equal to the Kruyt–Rothenburg strain.

2.2.5. The Cosserat strain of Kruyt

The above strains are based purely on the translations of particle centers. The microstructural interpretation of the Cosserat strain, introduced by Kruyt (2003), differs from all of them by taking into consideration the particle rotations as well. According to Eringen (1999), the 2D version of the Cosserat strain in a continuum is defined as

$$\mathrm{d}e_{ij} = \frac{\partial\, \mathrm{d}u_j}{\partial x_i} - \varepsilon_{ij}\,\mathrm{d}\omega, \tag{15}$$

where $\mathrm{d}u_j$ and $\mathrm{d}\omega$ are the translation and rotation of point x_i, and ε_{ij} is the 2D permutation symbol. To interpret this variable in a microstructural context, the equivalent continuum of the Kruyt–Rothenburg strain in Fig. 3 was modified: in the new version the boundary of the domain goes through those points ('boundary nodes') where the boundary grains are in contact with the external neighborhood of the ana-

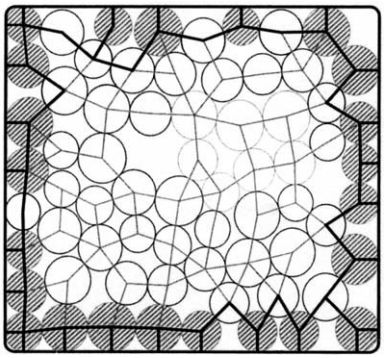

Fig. 6. The equivalent continuum of the Cosserat strain of Kruyt.

lyzed assembly (see Fig. 6, from Kruyt (2003)). So in addition to those polygons in Fig. 3, there are boundary polygons that lie within the domain and form its boundary. A boundary polygon contains a boundary branch (connecting two boundary nodes), and the 'centre' of a boundary polygon is defined as the midpoint of the boundary branch. Then the rotated polygon vector g_i^{pq} and the polygon vector h_i^{pq} are defined according to 2.2.3.

A continuous translation and rotation field can now be defined. Similarly to Section 2.2.3, let the translations and the rotations in the internal nodes of the equivalent continuum be equal to the translations and rotations of the corresponding particle centers. In the boundary node β, the translation $\mathrm{d}u_i^\beta$ and the rotation $\mathrm{d}\omega^\beta$ are the given displacements of β. Note that in case of non-deformable boundary contacts $\mathrm{d}u_i^\beta$ is determined from the displacements of that particle p which contains β

$$\mathrm{d}u_i^\beta = \mathrm{d}u_i^p - \varepsilon_{ij} r_j^{p\beta}\,\mathrm{d}\omega^p \tag{16a}$$

$$\mathrm{d}\omega^\beta = \mathrm{d}\omega^p, \tag{16b}$$

where $\mathrm{d}u_i^p$ is the translation of the centre of p and $\mathrm{d}\omega^p$ is the particle rotation, and $r_i^{p\beta}$ is the vector pointing from the particle centre to the boundary node β. In this case the rotation in the boundary node is also equal to the rotation of the corresponding particle. However, this is not a necessary requirement: the boundary contacts may be deformable, and in this case $\mathrm{d}u_i^\beta$ may be different from the right side of (16a), and $\mathrm{d}\omega^\beta$ may differ from $\mathrm{d}\omega^p$.

Finally, linear translation and rotation fields can be defined along all (internal and boundary) branches. It is assumed that there exist a continuous translation field and a continuous rotation field also in the interior of the polygons, but the fields are not defined in the interiors.

The area average of the Cosserat strain for a domain A is

$$\mathrm{d}\bar{e}_{ij} = \frac{1}{A}\oint_{(A)} \mathrm{d}e_{ij}\,\mathrm{d}A = \frac{1}{A}\oint_{(A)} \left(\frac{\partial\,\mathrm{d}u_j}{\partial x_i} - \varepsilon_{ij}\,\mathrm{d}\omega\right)\mathrm{d}A. \tag{17}$$

After long and complicated calculations, this could be expressed in a discrete form

$$\mathrm{d}\bar{e}_{ij} = \frac{1}{A}\sum_{(c)} \mathrm{d}v_j^c h_i^c. \tag{18}$$

Here $\mathrm{d}v_i^c$ is the relative translation at the contact point of branch c. If branch c is formed by particles p and q, then

$$\mathrm{d}v_i^c = \mathrm{d}v_i^{pq} = \left(\mathrm{d}u_i^q - \varepsilon_{ij} r_j^{qc}\,\mathrm{d}\omega^q\right) - \left(\mathrm{d}u_i^p - \varepsilon_{ij} r_j^{pc}\,\mathrm{d}\omega^p\right) \tag{19a}$$

as in (2); if the branch is formed by particle p and the boundary point β, then

$$\mathrm{d}v_i^c = \mathrm{d}v_i^{p\beta} = \mathrm{d}u_i^{\beta} - \left(\mathrm{d}u_i^p - \varepsilon_{ij} r_j^{p\beta} d\omega^p\right). \tag{19b}$$

The microstructural Cosserat strain of Kruyt in (18) differs from the Kruyt–Rothenburg strain in (11) in two respects:

- the equivalent continuum contains boundary polygons in addition to those polygons of the Kruyt–Rothenburg equivalent continuum;
- (18) contains the effect of particle rotations in addition to the particle translations, unlike (11).

2.3. Best-fit strains

The best-fit strains are based on finding that translation gradient tensor which gives the smallest deviation from the characteristic displacements of the system. The characteristic displacement can be the translations of particle centres, the relative translations at the contacts, etc. Depending on the kind of displacement to be approximated by an average translation gradient, different versions of best-fit strains are gained.

2.3.1. Cundall's best-fit strain

This approach was proposed by P.A. Cundall, and applied in the widely known softwares PFC and TRUBAL. Cundall's definition is valid for particles with arbitrary shape. The proposed definition is based on the translations of the particle centers, while the particle rotations are not taken into consideration.

Let x_i^p be the initial position of the centre of particle p at the beginning of the displacements. The translation of the centre of particle p is $\mathrm{d}u_i^p$. N^p is the number of all particles in the analyzed assembly. The average of the position vectors of particle centers is

$$x_i^0 = \frac{1}{N^p}\sum_{q=1}^{N^p} x_i^q, \tag{20}$$

and the average of the particle translations

$$\mathrm{d}u_i^0 = \frac{1}{N^p}\sum_{q=1}^{N^p} \mathrm{d}u_i^q. \tag{21}$$

The deviations of the individual particle positions can be calculated as

$$\tilde{x}_i^p = x_i^p - x_i^0, \tag{22}$$

while the relative translations of the individual particles with respect to the average translation are determined as

$$\mathrm{d}\tilde{u}_i^p = \mathrm{d}u_i^p - \mathrm{d}u_i^0. \tag{23}$$

Imagine that the assembly deforms in such a way that every particle translation exactly corresponds to a uniform translation gradient tensor α_{ij}. In this case we would find for the individual particle translations that they can be calculated from α_{ij} in the following way:

$$\mathrm{d}\tilde{u}_i^p = \alpha_{ji}\tilde{x}_j^p. \tag{24}$$

However, such a special situation usually does not happen, so in general cases we would find for any arbitrary α_{ij} that

$$\mathrm{d}\tilde{u}_i^p - \alpha_{ji}\tilde{x}_j^p \neq 0. \tag{25}$$

Now let us find that specific α_{ij} tensor for which the square sum of the deviations in (25) is the smallest (i.e. that α_{ij} which gives the 'best fit' to the particle translations)

$$Z = \sum_{p=1}^{N^p} (\mathrm{d}\tilde{u}_i^p - \alpha_{ji}\tilde{x}_j^p)(\mathrm{d}\tilde{u}_i^p - \alpha_{ji}\tilde{x}_j^p) \to \min \tag{26}$$

(the summation is carried out along all particles). The function Z is minimal at that α_{ij} for which

$$\frac{\partial Z}{\partial \alpha_{kl}} = 0 \tag{27}$$

for every (k,l). (It gives four equations in 2D, and nine equations in 3D.)

In 2D the four equations in (27) are written in details as

$$\begin{bmatrix} \sum_{p=1}^{N^p} \tilde{x}_1^p \tilde{x}_1^p & \sum_{p=1}^{N^p} \tilde{x}_2^p \tilde{x}_1^p \\ \sum_{p=1}^{N^p} \tilde{x}_1^p \tilde{x}_2^p & \sum_{p=1}^{N^p} \tilde{x}_2^p \tilde{x}_2^p \end{bmatrix} \begin{bmatrix} \alpha_{1i} \\ \alpha_{2i} \end{bmatrix} = \begin{bmatrix} \sum_{p=1}^{N^p} \mathrm{d}\tilde{u}_i^p \tilde{x}_1^p \\ \sum_{p=1}^{N^p} \mathrm{d}\tilde{u}_i^p \tilde{x}_2^p \end{bmatrix} \tag{28}$$

(i equals to 1 or 2).

The coefficient matrix on the left is always positive definite iff $N^p \geqslant 3$ and there exist at least three particles whose centers are not located along the same straight line. (The proof is given in Bagi (2005)). This is the sufficient and necessary condition of the existence of Cundall's best-fit strain in 2D.

From now, z_{ij} denotes the inverse of the coefficient matrix. Applying $i = 1$ in order to determine α_{11} and α_{21}, and $i = 2$ for the calculation of α_{12} and α_{22}, the solution of (28) can be written in the general form

$$\alpha_{ij} = z_{ik} \sum_{p=1}^{N^p} \mathrm{d}\tilde{u}_j^p \tilde{x}_k^p. \tag{29}$$

The tensor in (29), which minimizes the square sum in (26), is by definition the best-fit translation gradient of Cundall

$$\mathrm{d}\bar{e}_{ij} = z_{ik} \sum_{p=1}^{N^p} \mathrm{d}\tilde{u}_j^p \tilde{x}_k^p \quad (i,j,k = 1,2), \tag{30}$$

and its symmetric part is Cundall's best-fit strain.

In 3D the analysis is basically the same. Instead of the four equations in (28), the 3D analysis gives nine equations

$$\left(\sum_{p=1}^{N^p} \tilde{x}_n^p \tilde{x}_m^p \right) \alpha_{ni} = \sum_{p=1}^{N^p} \mathrm{d}\tilde{u}_i^p \tilde{x}_m^p \tag{31}$$

(n, m and i take the values 1, 2 and 3). The coefficient matrix on the left side of (31) is always positive definite iff $N^p \geqslant 4$ and there exist at least four particles whose centers are not located along the same plane. (The proof is also given in Bagi (2005)). This is the sufficient and necessary condition of the existence of Cundall's best-fit strain in 3D. Denoting the inverse of the 3×3 coefficient matrix $\sum_{p=1}^{N^p} \tilde{x}_n^p \tilde{x}_m^p$ by z_{ij} again, the best-fit

translation gradient can be calculated in the form given in (30), though the indices i, j, k now take the values 1, 2 and 3.

Note that this strain version does not take into account the particle rotations.

2.3.2. The best fit strain of Liao et al.

The best fit strain proposed by Liao et al. (1997) is based on a similar line of thought, but instead of the particle translations, its fundamental quantity is the contact deformations that can be determined from the particle translations and rotations. Let particle p the first and q the second grain forming contact c. The contact deformation, $\mathrm{d}v_i^c$, is given by (2).

If every particle would move exactly according to a uniform translation gradient α_{ij}, then the deformation at c would be

$$\mathrm{d}v_i^c = \alpha_{ji} l_j^c. \tag{32}$$

However, usually this is not the case, and for a general α_{ij} we would find that

$$\mathrm{d}v_i^c - \alpha_{ji} l_j^c \neq 0. \tag{33}$$

Similarly to the definition of the Cundall strain, let us find again that α_{ij} for which the square sum of the deviations in (33) is the smallest

$$Z = \sum_{c=1}^{M^c} (\mathrm{d}v_i^c - \alpha_{ji} l_j^c)(\mathrm{d}v_i^c - \alpha_{ji} l_j^c) \to \min \tag{34}$$

(the summation now includes all contacting pairs of grains in the assembly). The function Z becomes minimal at that α_{ij} for which

$$\frac{\partial Z}{\partial \alpha_{kl}} = 0 \tag{35}$$

for every (k, l). (Again, (35) gives four equations in 2D and nine equations in 3D.)

In 2D the four conditions in (35) are expressed in a system of linear equations that is rather similar to (28)

$$\begin{bmatrix} \sum_{c=1}^{M^c} l_1^c l_1^c & \sum_{c=1}^{M^c} l_2^c l_1^c \\ \sum_{c=1}^{M^c} l_1^c l_2^c & \sum_{c=1}^{M^c} l_2^c l_2^c \end{bmatrix} \begin{bmatrix} \alpha_{1i} \\ \alpha_{2i} \end{bmatrix} = \begin{bmatrix} \sum_{c=1}^{M^c} \mathrm{d}v_i^c l_1^c \\ \sum_{c=1}^{M^c} \mathrm{d}v_i^c l_2^c \end{bmatrix} \tag{36}$$

(i is 1 or 2).

The coefficient matrix on the left side of (36) is positive definite if there exist at least two branch vectors in the system that are not parallel to each other. This is the sufficient and necessary condition of the existence of the Liao et al. best-fit strain in 2D.

The nine equations in the 3D analysis can be summarized as

$$\left(\sum_{c=1}^{M^c} l_n^c l_m^c \right) \alpha_{ni} = \sum_{c=1}^{M^c} \mathrm{d}v_i^c l_m^c \tag{37}$$

(n, m and i can be 1, 2 or 3). The coefficient matrix in (37) is positive definite if there exist at least three branch vectors in the system that are not parallel to any common plane. This is the sufficient and necessary condition of the existence of the Liao et al. best-fit strain in 3D.

Let w_{ij} denote the inverse of the coefficient matrix in (36) or (37). The α_{ij} tensor that minimizes the square sum in (34) can be determined in the following way:

$$\alpha_{ij} = w_{ik} \sum_{c=1}^{M^c} \mathrm{d}v_j^c l_k^c. \tag{38}$$

This α_{ij} is the best-fit translation gradient of Liao et al.

$$\mathrm{d}\bar{e}_{ij} = w_{ik} \sum_{c=1}^{M^c} \mathrm{d}v_j^c l_k^c, \tag{39}$$

and its symmetric part is their proposed best-fit strain.

Note that the Liao et al. strain takes into account the particle rotations, unlike the Cundall strain.

2.3.3. The best-fit strains of Cambou et al.

Two improved versions of the Liao et al. strain were proposed by Cambou et al. (2000) (though their DEM analysis was restricted to 2D only, the theoretical results are valid also in 3D). Their first suggestion is to consider the relative translations $\mathrm{d}\Delta u_j^c$ instead of the contact deformations $\mathrm{d}v_i^c$ in the square sum in (34), which means to exclude the particle rotations from the analysis. The relative translation of the first particle p and second particle q forming contact c is simply

$$\mathrm{d}\Delta u_j^c = \mathrm{d}u_j^q - \mathrm{d}u_j^p. \tag{40}$$

Considering the contacting pair of grains (similarly to Liao et al. (1997)), the first best-fit translation gradient of Cambou et al. is

$$\mathrm{d}\bar{e}_{ij} = w_{ik} \sum_{c=1}^{M^c} \mathrm{d}\Delta u_j^c l_k^c, \tag{41}$$

where the tensor w_{ik} is the same as in (39). So the sufficient and necessary condition for the existence of the first best-fit strain of Cambou et al. is the same as for the Liao et al. strain.

Their second suggestion is to take into account not only the contacting, but also the neighboring pairs of grains. ('Neighboring' means such a pair for which the two particle centers are connected in the triangular system in Section 2.2.5.) Let M^e denote the number of all (contacting or neighboring) pairs of grains for which a branch exists in the triangular system; and let $\hat{w}_{ik}$ denote the inverse of the suitably modified coefficient matrices in (36) or (37). The second best-fit translation gradient tensor of Cambou et al. is

$$\mathrm{d}\bar{\bar{e}}_{ij}\hat{w}_{ik} \sum_{c=1}^{M^e} \mathrm{d}\Delta u_j^c l_k^c, \tag{42}$$

and its symmetric part is the proposed strain tensor. (Note that this version also excludes the particle rotations.)

The sufficient and necessary condition of the existence of the second best-fit strain of Cambou et al. is to have at least two neighboring pairs (at least three neighboring pairs in 3D) that are not parallel to each other (in 3D: they are not parallel to any common plane).

With the help of discrete element simulations Cambou et al. (2000) compared the Liao et al. strain and their first and second strain versions to the equivalent-continuum strain. Their first best-fit strain was closer to the equivalent-continuum strain than the version proposed by Liao et al., but still a significant deviation was found. On the other hand, the second best-fit strain showed an excellent agreement with the equivalent-continuum strain.

2.4. The Satake strain

The microstructural strain definition of Satake (2004) is valid for assemblies of circles or spheres. At first sight it seems to be an equivalent-continuum strain just like those in Section 2.2, since it is also based on a tessellation system ('contact cells'). But the Satake strain is basically different from the equivalent-continuum strains, since there is no continuous translation field assigned to the contact cells, and no cell deformations are analyzed.

The geometrical background of the definition is based on the generalized Dirichlet–tessellation (Fejes Toth, 1953) that is shown in thick lines in Fig. 7. The generalized Dirichlet cell belonging to particle p is formed by those points of the space that have a shorter or equal tangent section to particle p than to any other particle. The points along a common face of two neighboring cells have an equal tangent length to the two circles/spheres (so the common faces are the power lines/power planes of the two grains). This cell system is also called Laguerre tessellation (Okabe et al., 2000).

The Delaunay-cells (thin lines in Fig. 7) are formed by the branches connecting those centers of particles that have a common face in the generalized Dirichlet–tessellation. (Note that the Delaunay-branch is always perpendicular to the corresponding Dirichlet-face.) The nodes of this system are the particle centers, and the branches correspond to contacting or neighboring pairs of particles.

Based on these two tessellations, Satake defined the *contact cells* (see the 2D version in Fig. 8). A contact cell belongs to a pair of neighboring or contacting grains. The cell is determined by the face of the generalized Dirichlet-system, and by the corresponding Delaunay-branch.

Consider the contact cell of the AC pair. The corresponding branch vector is l_i^{AC}. The vector $\hat{h}_i^{AC}$ belongs to the face between A and C. Its direction is perpendicular to the face, and its magnitude is equal to the length (2D) or area (3D) of the face. The area (2D) or volume (3D) of the contact cell is calculated as

$$A^{AC} = \frac{1}{2}(l_k^{AC}\hat{h}_k^{AC}) \quad \text{in } 2D, \tag{43a}$$

$$V^{AC} = \frac{1}{3}(l_k^{AC}\hat{h}_k^{AC}) \quad \text{in } 3D. \tag{43b}$$

From now on, the scalar D denotes the dimension of the analysis.

Consider now contact cell e. The second particle, q, expresses f_i^e contact force on the first particle of the contact, p. The contact deformation, $\mathrm{d}v_i^e$, is calculated from the particle displacements according to (2). The stress tensor σ_{ij}^e and the translation gradient tensor $\mathrm{d}e_{ij}^e$ are, by definition, equal to

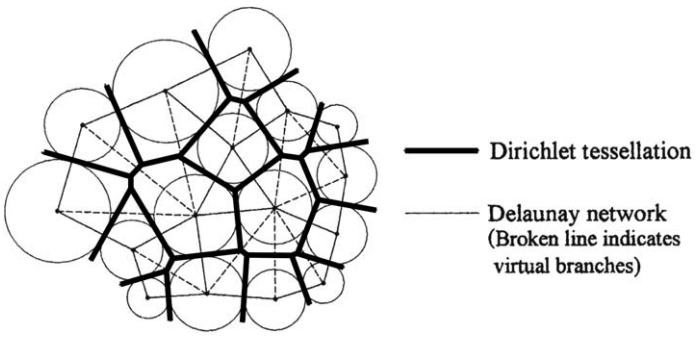

Fig. 7. The generalized Dirichlet–tessellation and the corresponding Delaunay-cells.

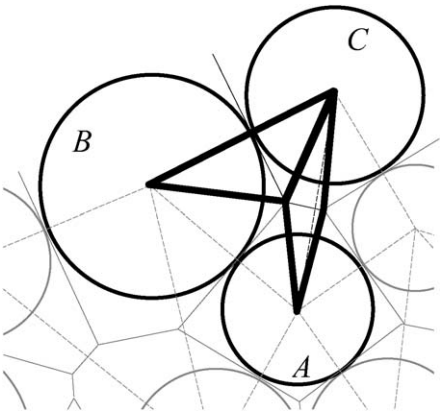

Fig. 8. The contact cells of Satake: an internal cell belonging to branch AC, and a boundary cell belonging to branch BC.

$$\sigma_{ij}^{e} = \frac{1}{2A^{e}} l_i^{e} f_j^{e} \quad \text{if } D = 2, \quad \text{and} \quad \sigma_{ij}^{e} = \frac{1}{3V^{e}} l_i^{e} f_j^{e} \quad \text{if } D = 3, \tag{44}$$

$$\mathrm{d}e_{ij}^{e} = \frac{1}{2A^{e}} \hat{h}_i^{e} \,\mathrm{d}v_j^{e} \quad \text{if } D = 2, \quad \text{and} \quad \mathrm{d}e_{ij}^{e} = \frac{1}{3V^{e}} \hat{h}_i^{e} \,\mathrm{d}v_j^{e} \quad \text{if } D = 3. \tag{45}$$

By assuming small particle displacements, the increment of the internal work is

$$\mathrm{d}W = \sum_{(e)} (f_k^{e} \,\mathrm{d}v_k^{e}) = \sum_{(e)} (l_k^{e} \hat{h}_k^{e})(\sigma_{ij}^{e} \,\mathrm{d}e_{ij}^{e}). \tag{46}$$

(The summation is done for all contact cells.)

The average translation gradient of the whole system is, by definition, given by

$$\mathrm{d}\bar{e}_{ij} = \frac{1}{\sum_{(e)} A^{e}} \sum_{(e)} \hat{h}_i^{e} \,\mathrm{d}v_j^{e} \quad \text{if } D = 2, \quad \text{and} \quad \mathrm{d}\bar{e}_{ij} = \frac{1}{\sum_{(e)} V^{e}} \sum_{(e)} \hat{h}_i^{e} \,\mathrm{d}v_j^{e} \quad \text{if } D = 3. \tag{47}$$

The symmetric part of $\mathrm{d}\bar{e}_{ij}$ is the microstructural strain tensor defined by Satake.

In spite of the theoretical beauty and importance of this variable, since the generalized Dirichlet–tessellation has to be compiled for the system, and the vectors $\hat{h}_i^{e}$ have to be exactly determined, the numerical calculation of this strain version is very time-consuming and may hinder their immediate application.

3. Discrete element simulations

The aim of the numerical analysis was to compare the different microstructural strain versions with the overall, macro-level deformations. The simulations were performed with the help of PFC-2D (Itasca, 2002), a discrete element software based on the 2D dynamical Cundall model (Cundall and Strack, 1979). The analyzed assemblies consisted of circular particles located in a square domain surrounded by four straight walls.

The following microstructural strain versions were analyzed:

- the Bagi strain;
- the Kruyt–Rothenburg strain;
- the Liao et al. best-fit strain;

- Cundall's best-fit strain;
- the microstructural Cosserat strain of Kruyt.

The following strains were *not* measured in the tests:

- the equivalent-continuum strains of Kuhn and of Cambou et al., since these are equal to the Kruyt–Rothenburg strain;
- the two best-fit strains of Cambou et al., since there are convincing numerical simulations about their behavior in Cambou et al. (2000);
- the Satake-strain, because of the enormous computational cost associated with the preparation of the contact cells.

Three small assemblies and one large assembly was generated with the help of the Inwards Packing Method (Bagi, 2005). The small assemblies consisted of 1037, 1040 and 1035 circular grains, all of them located in a 30 cm × 30 cm square domain. The large assembly contained 16,571 grains and the surrounding square was 120 cm × 120 cm. The grain size distribution was the same in all cases. The particle diameters were as follows:

30% 0.5 – 0.8 cm
38% 0.8 – 1.0 cm
26% 1.0 – 1.3 cm
6% 1.3 – 1.5 cm.

The generated assemblies were compacted by moving the walls inwards until the porosity reached the value of 13.1%. At this stage the domain sizes were 29.2803 cm × 29.2803 cm and 117.1212 cm × 112.1212 cm at this stage.

The contacts were linearly elastic, with an equal normal and shear stiffness of 10^4 N/cm. Two different friction coefficients (f) were applied: the above assemblies were tested with $f = 0.2$, and then the tests were repeated with $f = 0.01$.

By slowly translating the walls, two different kinds of deformations were produced in the tests (see Fig. 9 as well):

(a) uniaxial compression, by translating the bottom and top walls towards each other, until 1% vertical contraction;
(b) biaxial shear, by vertically compressing and horizontally extending the domain, until 1% strain was produced in both directions.

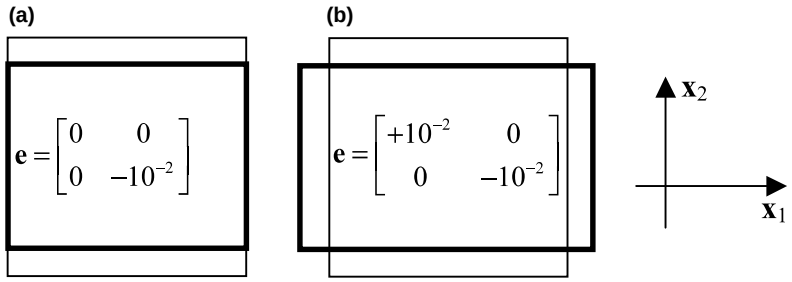

Fig. 9. Prescribed deformations of the surrounding domain: (a) uniaxial compression and (b) biaxial shear (the figures contain the final macro-level strains).

The *macro-level deformation* was understood as the deformation of the original square domain surrounded by the walls. The microstructural strains were compared to this deformation.

The equivalent-continuum strains were determined in the following way:

The Bagi strain was calculated with the help of the boundary integral (8), along the boundary line illustrated in Fig. 2. The Kruyt–Rothenburg strain was also determined with the help of a boundary integral that was carried out along the boundary shown in Fig. 3. In order to get the Cosserat strain of Kruyt, the displacements of the boundary points were defined according to (16). Then (18) was applied in order to calculate the average Cosserat strain.

The two best-fit strains were calculated according to (30) and (39).

The simulation results are illustrated in Figs. 10 and 11:

- On any diagram, the horizontal axis shows a component of the macro-level deformation (e.g. e_{11} in Fig. 10a and c, e_{22} in Fig. 10b and d). The total strain, 1%, was produced in ten equal deformation steps, and after every step the characteristic components of the different strain versions were determined. The values from 1 to 10 on the horizontal axes indicate these steps.
- The vertical axis measures the ratio of the different microstructural strains related to the macro-strain. (If a microstrain would exactly be equal to the macro-strain, the value 1.00 should be measured vertically.)

The simulation results show that the equivalent-continuum strains of Bagi and of Kruyt and Rothenburg were close to the macro-level deformations in all tests, and they were also close to each other. Even in the worst cases the deviations hardly reached a few percent of the macro-strain.

A clear size effect could be detected in both strain versions. Comparing the results of the large and of the small assemblies, the strains of Bagi and of Kruyt-Rothenburg was closer to the macro-strain in case

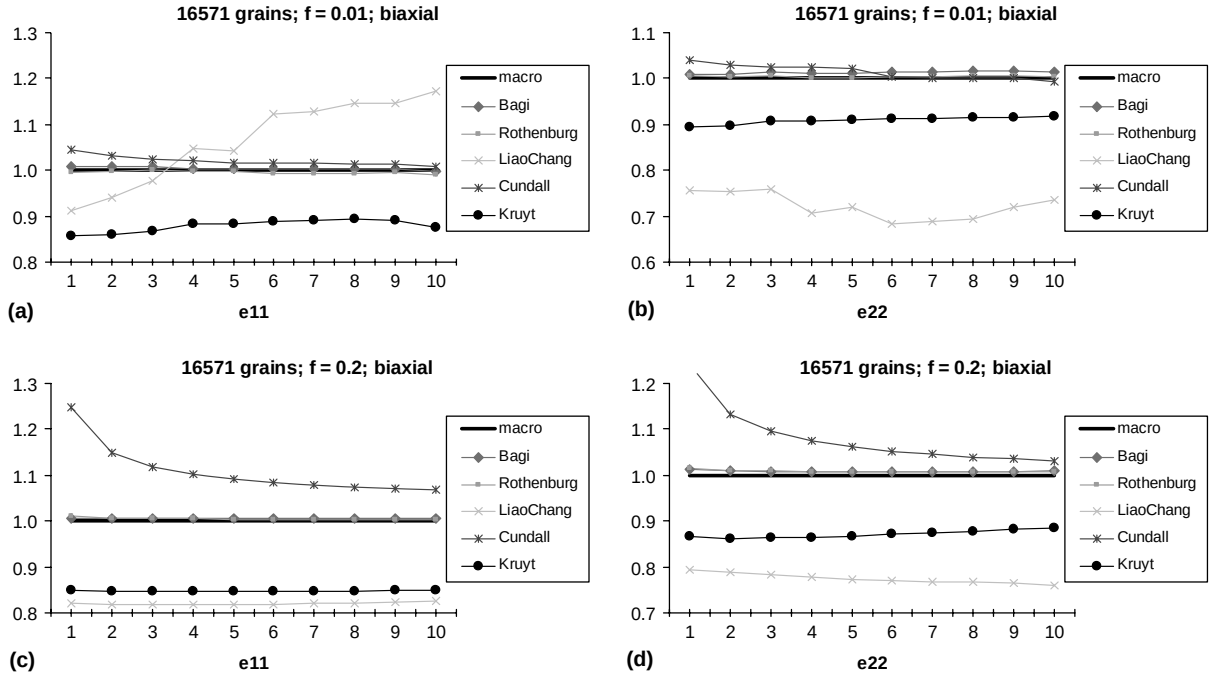

Fig. 10. Biaxial tests on the large assembly: (a) and (b): frictionless; (c) and (d): frictional grains.

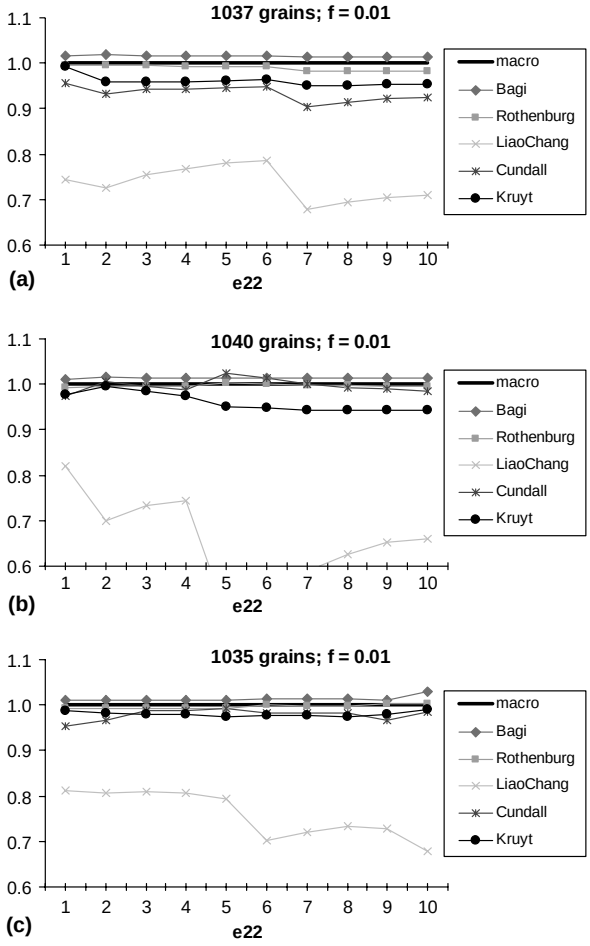

Fig. 11. Uniaxial tests on small frictionless assemblies.

of the large assembly than in case of the small assemblies. The reason of this size effect is that in both strain versions the strain is measured within a domain whose boundary goes through the centres of boundary particles, while the macro-strain is measured in a domain whose boundary goes through the boundary contacts of the same particles. As the number of particles in the assembly increases, the relative thickness of this layer (compared to the domain size) decreases. (In case of the other variables such an effect could not be noticed.)

The best-fit strain of Cundall was not reliable: in many cases it was in a good agreement with the macro-strain, but sometimes the deviation was rather significant, 20–30%. The reasons of the deviations are not clear yet: further investigations are necessary on the issue.

The Liao et al. strain significantly differed from the macro-strain in most cases (the deviation often reached or exceeded 40–50% of the macro-strain).

The microstructural Cosserat strain of Kruyt always under-estimated the macro-strain: in the uniaxial tests the difference was usually around a few percent, while in the biaxial tests it often reached 10–15% (this is probably the result of the more significant particle rotations in the biaxial tests).

4. Summary

The paper focused on the theoretical and numerical analysis of the different microstructural strain tensors. Ten different versions were introduced and compared, by theoretical and numerical investigations. The following results were found:

- The Kruyt–Rothenburg strain and the Bagi strain were in good agreement with the macro-level deformations in discrete element simulations. (The former can be applied only in 2D, though it is more easy to calculate.)
- The strain of Kuhn and the equivalent-continuum strain of Cambou et al. are equal to the Kruyt-Rothenburg-strain, so they are also suitable for the description of the overall deformations in 2D.
- Among the best-fit strains, in the case of frictionless particles the strain of Cundall was nearly as close to the macro-deformations in DEM simulations as the previous strain versions. The advantages of the Cundall strain are its calculational simplicity, and its validity in 3D.
- Numerical results in the literature show that the 2nd best-fit strain of Cambou et al. is also very close to the macro-level deformations. Its disadvantage is that the triangularization of the granular system makes the strain calculations much more time-consuming than in the case of the Cundall strain.
- The simulations in the present paper confirmed the results of Cambou et al. (2000) that the best-fit strain of Liao et al. did not give a good estimation of the macro-deformations.
- The microstructural Cosserat strain of Kruyt was close to the macro-deformations in uniaxial compression tests, but significantly under-estimated them in biaxial tests.

Acknowledgements

This work was supported by the OTKA project # 34771. The valuable comments of N.P. Kruyt are greatly acknowledged.

References

Bagi, K., 1993. On the definition of stress and strain in granular assemblies through the relation between micro- and macro-level characteristics. Powders and Grains 93, Thornton Balkema, C. (Ed), pp. 117–121.

Bagi, K., 1995. Geometrical modeling of granular assemblies. Acta Technica Acad. Sci. Hung. 107 (1-2), 1–16.

Bagi, K., 1996. Stress and strain in granular assemblies. Mech. Mater. 22, 165–177.

Bagi, K., 2005. Dissertation for the DSc degree, Hungarian Academy of Sciences, Budapest.

Bagi, K., 2005. An algorithm to generate random dense arrangements for discrete element simulations of granular assemblies. Granular Matter 7, 31–43.

Cambou, B., Chaze, M., Dedecker, F., 2000. Change of scale in granular materials. Eur. J. Mech. A/Solids 19, 999–1014.

Cundall, P.A., Strack, O.D.L., 1979. A discrete numerical model for granular assemblies. Geotechnique 29, 47–65.

Dedecker, F., Chaze, M., Dubujet, Ph., Cambou, B., 2000. Specific features of strain in granular materials. Mech. Cohesive-Frictional Mater. 5, 173–193.

Eringen, A.C., 1999. Microcontinuum Field Theories: Foundations and Solids. Springer-Verlag, New York.

Fejes Toth, L., 1953. Lagerungen in der Ebene auf der Kugel und im Raum. Springer-Verlag, Berlin.

Holzapfel, G., 2001. Nonlinear Solid Mechanics. Wiley & Sons, Chichester, pp. 70–84.

Itasca, C.G., 2002. PFC-2D, Particle Flow Code in 2 Dimensions. Theory and Background. Itasca, 708 South Third Street 310, Minneapolis, 55415 USA.

Kruyt, N., Rothenburg, L., 1996. Micromechanical definition of the strain tensor for granular materials. J. Appl. Mech. 118, 706–711.

Kruyt, N.P., 2003. Statics and kinematics of discrete Cosserat-type granular materials. Int. J. Solids Struct. 40, 511–534.

Kuhn, M., 1997. Deformation measures for granular materials. In: Proc. Mechanics of Deformations and Flow of Particulate Materials, 29 June–02 July 1997, Evanston, pp. 91–104.

Kuhn, M., 1999. Structured deformation in granular materials. Mech. Mater. 31, 407–429.
Liao, C.L., Chang, T.P., Young, D.H., Chang, C.S., 1997. Stress–strain relationship for granular materials based on the hypothesis of best fit. Int. J. Solids Struct. 34, 4087–4100.
Okabe, A., Boots, B., Sugihara, K., Chiu, S.N., 2000. Spatial Tessellations. Wiley & Sons.
Rothenburg, L., 1980. Micromechanics of idealized granular materials. PhD Dissertation, Carleton University, Ottawa, Canada.
Satake, M., 2004. Tensorial form definitions of discrete mechanical quantities for granular assemblies. Int. J. Solids Struct. 41, 5775–5791.